Dynamics of Serine-8 Side-chain in Amyloid-β fibrils and Fluorenylmethyloxycarbonyl Serine Amino Acid, Investigated by Solid-State Deuteron NMR

Liliya Vugmeyster^{†,*}, Dan Fai Au[†], Dmitry Ostrovsky[‡], Dillon Ray Lee Rickertsen[†], Scott M. Reed[†]

Keywords: deuterium NMR, solid-state NMR, amyloid fibrils, disordered domains, protein dynamics

Abstract

Serine side-chains are strategic sites of post-translational modifications and it is important to establish benchmarks of their internal dynamics. In this work we compare the dynamics of serine side-chains in several biologically important systems: Serine-8 in the disordered domain of $A\beta_{1-40}$ fibrils in the hydrated and dry states and fluorenylmethyloxycarbonyl(Fmoc) serine with the bulky group that mimics hydrophobicity of the fibrils contacts yet lacks the complexity of the protein system. Using deuterium solid-state NMR static line shape and longitudinal relaxation techniques in the 310 to 180 K temperature range, we compare the main features of the dynamics in these systems. The main motional modes in the fibrils are large-scale fluctuations in the hydrated state of the fibrils, as well as local motions such as 3-site jumps of the C^{β} deuterons at high temperatures and small-angle fluctuations of the C^{α} - C^{β} axis at low temperatures. In the hydrated fibrils two distinct states are present with vastly different extent of large scale diffusive motions and 3-site jumps rate constants. The hydrated state at the physiological conditions is dominated by the "free" state undergoing large-scale diffusive motions and very fast local 3-site jumps, while in the

[†] Department of Chemistry, University of Colorado Denver, Denver CO USA 80204

[‡] Department of Mathematics, University of Colorado Denver, Denver CO USA 80204

^{*}To whom correspondence should be addressed: 1201 Larimer Street, Denver CO 80204, USA email: <u>LILIYA.VUGMEYSTER@UCDENVER.EDU</u>

"bound" state these large scale motions are quenched due to transient inter- and intra-molecular interactions. Additionally, in the bound state the 3-site-jump motions are orders of magnitude slower. Details of the dynamics in the serine side-chain are dependent on fine structural features and hydration levels of the systems.

Amyloid-β fibrils (Aβ) fibrils are hallmarks of the Alzheimer's disease. Aβ fibrils consist of a

Introduction

structured hydrophobic core and a flexible N-terminal domain.¹⁻³ Aß protein in its monomeric, fibrillular and oligomeric forms has been studied by a huge variety of biophysical techniques in an attempt to uncover the molecular basis of the disease, which still remains somewhat of a mystery.⁴⁻ ⁶ A recent focus of our group is the flexible N-terminal domain of $A\beta_{1-40}$ protein in the fibrillar form, which contains a number of sites important in aggregation control.⁷⁻¹⁴ One of the ways this control can be established is by virtue of post-translational modifications. ¹⁵ Serine-8 is one of the important phosphorylation sites in AB: upon phosphorylation, fibrils' structure and dynamics, as well as the aggregation propensity and kinetics of fibril formation are significantly altered. ¹⁶ In this work we utilized deuterium NMR in order to compare the dynamics of the wild-type $A\beta_{1-40}$ fibrils in the 3-fold symmetric polymorph¹⁷ deuterated at the side-chain of S8 with those of the Nfluorenylmethyloxycarbonyl(Fmoc)-L-serine amino acid (Figure 1). The comparison permits us to discern features unique to the protein fibrils system and not just the serine side-chain in the hydrophobic environment in Fmoc-serine. We have previously employed deuterium NMR to look at the dynamics of other sites in the flexible N-terminal domain^{18, 19} and this study also places the results for the S8 position in the context of these studies.

The N-terminal domain of the fibrils has been shown to undergo extensive conformational rearrangements, ^{14, 20} which could be modeled as the large-scale diffusive motion and the two-site exchange between the "free" and the "bound" states of the domain. In the bound state the N-terminal domain remains rigid due to inter or intra-molecular interactions with the structured fibrils core or neighboring chains. In particular, we have previously probed the dynamics at the side-chains of A2, F4, τ -H6, G9, and V12 sites. The large-scale diffusive motion defines static deuterium line shapes at these sites, while local motional modes can be probed with longitudinal relaxation measurements.

For the site-specific studies of side-chain dynamics with the use of deuterium solid-state NMR, selective deuteration of the sites is required. This is often limited by commercially available isotopic labeling patterns and availability of amino acids with protection groups necessary for the solid-state peptide synthesis. In this work, we utilized synthetic approaches to incorporate the side-chain protection group into the commercially available Fmoc-serine- $C^{\alpha}D$ - $C^{\beta}D_2$ amino acid, which subsequently allowed for the solid-state peptide synthesis of the $A\beta_{1-40}$ protein with the deuterium label at the S8 site.

We conduct a detailed quantitative characterization of global and local dynamical modes of the serine side-chains in the hydrated and dry fibrils and in Fmoc-serine. In particular, we determine the rate constants and diffusion coefficients at high temperatures close to the physiological conditions and activation energies of motions from the temperature-dependence of the longitudinal relaxation data. The most relevant local motional mode in the high temperature regime is the 3-site jumps of C^{β} deuterons with variable populations depending on the state of the fibrils. Due to a significant role that serine side-chains play in post-translational regulations across a wide range of protein systems, the importance of our study lies in the expansion of tools for determination of the dynamics and assessment of the ranges of expected parameters for serine-containing systems.

Materials and Methods

Preparation of Aβ1-40 peptide and fibrils: The peptide was prepared using solid-state peptide synthesis (performed by Thermofisher Scientific Co, Rockford, IL). The native sequence is DAEFRHDSGYEVHHQKLVFFAEDVGSNKGAIIGLMVGGVV. In brief, *N*-Fmoc -L-serine-2,3,3-d₃-trityl was synthesized starting from Fmoc -L-serine-2,3,3-d₃, which was purchased from CDN Isotopes (Quebec, Canada), following procedures similar to Krawczyk et al. ²¹ Conversion to an ester was accomplished by reaction with benzyl bromide in a 84% yield. Addition of trityl chloride followed by hydrogenolysis with H₂ over Pd/C at an overall yield of 36%. Supporting Information SI1 describes the details of the synthetic procedure. The identity of the product was confirmed by solution 1 H and 13 C NMR as well as by mass spectrometry. Fibrils of the wild-type Aβ₁₋₄₀ in the "twisted/3-fold" polymorhps were produced using established seeded growth protocols under quiescent conditions. 1,19,22 The morphology was confirmed by negatively stained transmission electron microscopy (Figure 1D). 15 mg of dry fibrils were obtained. A hydrated state with water content of 2 μ l of water per 1 mg of protein was achieved by pipetting 30 μ l of deuterium depleted H₂O, mixing it into the fibrils and equilibrating for 4 days.

Deuteron Solid-state NMR spectroscopy: Experiments under static conditions were performed using a 9.4 T spectrometer equipped with a static 5 mm Phoenix probe. Line shape experiments were performed with a quadrupole echo pulse sequence based on an eight-step phase cycle,²³ with the echo delay of 36 μs. The number of scans varied from 128 to 4096 depending on sensitivity of each sample and fraction of the bound state in the hydrated fibrils. The exponential line broadening function of 0.5 to 2 kHz was employed to enhance the signal to noise ratio. Longitudinal relaxation measurements under static conditions were performed using the inversion recovery sequence for relaxation times below 80 ms and saturation recovery sequence for longer times. The durations of

90° pulses were 2.0 μs. Six to ten relaxation delays were collected. Experiments at the MAS conditions were performed using a 18.8 T spectrometer equipped with a tri-gamma probe at 25 kHz spinning rate and set point of 295 K, corresponding to the sample temperature of around 312 K. A 90° pulse length of 4 μs was employed and longitudinal relaxation measurements were done using the inversion recovery sequence.

Motional modeling

Modeling of the S8-A β_{1-40} line shapes in the hydrated fibrils according to the isotropic diffusion mode was performed as described in previous work.¹⁹ Briefly, the isotropic diffusion of the free state was modeled as discrete nearest-neighbor jumps on the surface of a sphere, using 192 sites with the DistMesh program²⁴ for the discretization of the Smoluchovski equation. The jump rate was the same for all pairs of sites and was selected to match the second non-zero eigenvalue of the diffusion operator (corresponding to the second-order Legendre polynomial eigenfunction) to be 6D. The effective tensor in the fast motional limit of 3-site jumps of C^{β} deuterons was modeled with the quadrupolar coupling constant $C_q = 53$ kHz and the asymmetry parameter $\eta = 0$.

The spin-lattice relaxation rate T_l is given by 23,25

$$\frac{1}{T_1} = \frac{C_q^2}{3} \left(J_1(\omega_0) + 4J_2(2\omega_0) \right) \tag{1}$$

where ω_0 is the Larmor frequency, J_1 and J_2 are spectral density functions, and C_q is the quadrupole coupling constant in the absence of motion. J_1 and J_2 are dependent on the timescales and types of underlying motional processes as well as on the crystallite orientations. Spectral density functions can be obtained analytically for several simple models of motion. However, a description of the processes with multiple motional modes and/or multiple conformers usually requires computer simulations. Modeling of the 3-site jumps of the C^{β} deuterons group involved tetrahedral geometry

with the angle of 109.5° between C^{α} - C^{β} axis and the direction of the C^{β} -D bonds with one major site and two equal minor sites with populations in w:1:1 ratio. For the free state of the hydrated fibrils, the three rotamers were modeled with equal weights. Small-angle fluctuations were modeled as two-site jumps of $\pm 5^{\circ}$ amplitude around the χ_1 dihedral angle. We assume that the principal axis system of the quadrupolar tensor for each deuteron is aligned along the position of the C-D bond and employ the value of $C_q = 159$ kHz.

The temperature dependence of the rate constants for large- and small-angle jumps in each conformer is taken to be Arrhenius: $k(E_a^{3-site},T)=k_o^{3-site}e^{-E_a^{3-site}/T}$ and $k(E_a^{small},T)=k_o^{small}e^{-E_a^{small}/T}$. The populations factor w is assumed to follow the Boltzmann law: $w=e^{-\Delta E/RT}$ where ΔE is the energy difference between the major and minor rotamers. As explained in the Results and Discussion section due to non-exponentiality of the magnetization build up curves, the full model involves distributions of conformers distinguished by different value of their activation energies. For the 3-site jumps mode, the distribution is taken with respect to the height of the barrier between the major and minor rotamers, with the energy difference ΔE between rotamers remaining the same for all conformers. The values of k_o^{3-site} and k_o^{small} were assumed to be the same for all conformers. For the case of a continuous distribution of conformers magnetization M(t) is defined by

$$M(t) = \iint m(E_a^{3-site}, E_a^{small}, t) dE_a^{3-site} dE_a^{small}$$
 (2)

in which $m(E_a^{3-site}, E_a^{small}, t)$ is the magnetization density. The magnetization density is proportional to the distribution functions for the activation energies.²⁷ The distributions are assumed to have Gaussian shapes and are parametrized by the central values of $\langle E_a^{3-site} \rangle$ and $\langle E_a^{small} \rangle$ and the widths of σ_{3-site} and σ_{small} respectively. In simulations, the continuous

distribution is approximated by 11 discrete conformers in each dimension. The obtained M(t) profiles were fitted by the stretched-exponential function defined in Eq. (3) to yield simulated values of T_1^{eff} and β . Thus, a library of simulated parameters T_1^{eff} and β was created as a function of the small- and large-angle jump rates in order to fit the experimental data for Fmoc-serine. Modifications of the approach for the fibrils samples is described in the Results and Discussion section. The fitting was performed using χ^2 minimization and the uncertainties were estimated by the inverse covariance matrix method.

Results and Discussion

Sample conditions, labeling patterns, and spectral analysis

Fmoc-serine used in this work has deuterium labels at both C^{α} and C^{β} positions (Figure 2A). However, the C^{α} site is expected to be significantly more rigid and can be effectively excluded with the use of a short inter-scan delay. ²H magic-angle spinning (MAS) measurements at 18.8 T and 25 kHz spinning rate did not differentiate between the two sites with inter-scan delays as large as 600 s. (Figure 2, top panel). The expected chemical shift values calculated with nmrdb.org program²⁸ are around 3.6 ppm for C^{α} and 4.5 ppm for C^{β} deuterons, respectively. Based on these values, the two peaks should likely lead to a very asymmetric total resonance within our resolution of about 1.5 ppm, if their intensities were proportional to the number of the corresponding deuterium nuclei. Further, relaxation times measurements with the relaxation delays up to 5 s did not display significant anisotropy across the center band region, which would be expected in the presence of two distinct sites. (Figure 2, bottom panel). Thus, we conclude that the C^{α} deuterons in Fmoc -serine are very rigid with relaxation times significantly larger than 10 min and the signal originates almost entirely from the C^{β} deuteron. Static deuterium spectrum collected with the

quadrupolar echo pulse sequence²³ (Figure 3A) indicates a rigid powder pattern with the distance between the major singularities of 118-119 kHz across the entire temperature range of 330 K to 178 K. This distance translates to the C_q value of 159 kHz.

In order to incorporate Fmoc-serine into the AB peptide, solid-state peptide synthesis requires a protection group of the side-chain in addition to the amide Fmoc protection group. We have used synthetic procedures outlined in the materials and methods and Supporting Information (SI1, Figure S1) to incorporate the trityl protection group. The resulting fibrils had deuterium labels at C^{α} and C^{β} positions. Unlike Fmoc-serine itself, the spectrum for the hydrated fibrils at 310 K has two components (Figure 3C): the major component is strikingly narrow, indicating large-angle rearrangements of the side-chain, and a moderate rigid-like component is also visible with about 20-22% fraction based on the spectral decomposition (Figure S2). This is in agreement with previous measurements on other selected sites of the N-terminal domain. ¹⁹ The large scale motions can be approximated by isotropic diffusion for a relative comparison between the residues. They gradually freeze out from the N-terminal end site A2-CD3 toward the V12-CD3 site, with the latter displaying the spectrum indicative of the absence of the large-scale diffusive motion. This narrowing is only observed for the hydrated fibrils, while the dry fibrils display the rigid-like patterns close to that of Fmoc-serine (Figure 3B). The presence of the rigid fraction in the spectrum (see insert for the 310 K spectrum of hydrated S8-labled fibrils in Figure 3C) indicates that a fraction of the fibril does not participate in the large-angle fluctuations. Thus, in the simplest model we have postulated two states of the N-terminal domain (Figure 4): the free state undergoing largescale rearrangements (approximated by the isotropic diffusion) and the bound state in which the motions are quenched due to intra and inter-molecular interactions with the core of the fibrils and neighboring N-terminal ends from different chains of the stacked fibrils. 19 As the temperature is lowered, the relative fraction of the wide powder-pattern increases (see Figure 3D for an example

spectrum for S8 and previous work for detailed spectra for other residues¹⁹), indicating that the fraction of the bound state increases. Further, we have shown that at the physiological temperature the two states are in slow exchange conformational regime with the rate constants that can be quantified by 2 H R_{1p} and QCPMG relaxation measurements. This work will not focus on this conformational exchange mode.

The central narrow component of the line shape of the hydrated fibrils at 310 K can be modeled with the isotropic diffusion coefficient D of $4.8 \cdot 10^5$ rad²/s (Figure S2), which falls in between $D = 7 \cdot 10^5$ rad²/s for H6 and $3.4 \cdot 10^5$ rad²/s for G9, determined previously. The bound fraction of 20% also falls within the previously determined sequence along the N-terminal chain, which is 10% for H6 and 35% for G9. The agreement across all residues in the relative values of the diffusion coefficient can only be obtained if the motionally narrowed tensor with the C_q value of 53 kHz is used for the simulations of S8 side-chain motions. These values imply that the 3-site jumps of the C^β deuterons are in the fast motional limit with respect to the quadrupolar coupling constant and there is no preferred population between the three rotameric positions of the C^β deuterons of S8 in the free state of the hydrated fibrils. As we will see below, the longitudinal relaxation data also confirm this assumption.

²H NMR Longitudinal Relaxation behavior defines local motions

I. Fmoc-serine

Longitudinal T_1 relaxation behavior is governed by motions of the order of Larmor frequency (67 MHz at 9.4 T), and originates from local motional modes at the labeled sites. In Fmoc -Serine, there are two potential sources of relaxation for the C^{β} deuterons: the 3-site jumps according to the tetrahedral geometry and small angle fluctuations of C^{α} - C^{β} axis (Figure 4A). As the relaxation

times (Figure 5 and 6) do not display a simple Arrhenius behavior (i.e., $\log T_1$ is not linear with 1/T), the presence of both mechanisms is implied. At high temperatures the 3-site-jump mechanism is expected to dominate relaxation due to a higher efficiency, while at low temperatures, when the rate of the 3-site jumps slows down significantly, small-angle fluctuations provide an alternative mechanism. Both mechanisms are thermally activated processes but with clearly different values of the activation energies. The small-angle fluctuations are expected to yield much lower values of the activation energies based on the observed leveling out of the relaxation times at low temperatures.

Rotameric libraries^{29, 30} for the serine side-chains in proteins indicate somewhat different populations of the three rotamers around the χ_1 dihedral angle, as would be expected in the presence of the OH group. We started with the assumption of equal populations and could not reconcile the line-shape data with the relatively fast relaxation times at high temperature (Figure S3). The 3-site jumps rate constant consistent with the relaxation times at high temperatures would indicate a motionally narrowed line shapes in intermediate regime with respect to C_q value of 159 kHz, in comparison to the rigid pattern observed experimentally. This discrepancy disappears with introduction of unequal populations of the three sites, with the simplified assumption of one major and two minor populations in w:1:1. Further breakdown into three unequal populations is not necessary within the precision of the data. The assumption of tetrahedral geometry is another approximation and deviations from this assumption can be expected in the presence of the OH group, but this does not change the overall qualitative interpretation of the data within its precision. The potential including the two modes in shown in Figure 4C. Small-angle fluctuations were taken with 10° amplitude. The exact amplitude of these fluctuations is not significant for the physical interpretation of the results. Both mechanisms are thermally activated and we assume that the Arrhenius law holds for the temperature dependence of the rate constants and Boltzmann law for

the temperature dependence of the populations, with ΔE defining the energy difference between the major and the minor rotamers and E_a^{3-site} defining the activation energy barrier between the rotamers. E_a^{small} defines the activation energy barrier for the small-angle fluctuations.

The magnetization build-up curves (Figure 5, shown for the major singularities of the powder pattern) are in general not single-exponential across the entire temperature range, implying that at each temperature for each mechanism there is a distribution of rate constants, originating from inhomogeneity of the local environment. This type of non-exponential magnetization build up curves can be fitted well with the use of stretched-exponential function of the form:³¹

$$M(t) = M(\infty)(1 - e^{-(t/T_1^{eff})^{\beta}})$$
(3)

in which M(t) is the signal intensity, T_1^{eff} is the effective relaxation time, and β is the parameter which reflects the degree of non-exponentiality, $0 < \beta < 1$. β less than 1 corresponds to a non-exponential behavior. Eq. (3) is one of the typical empirical functions that are used in descriptions of various dynamic effects in glasses. $^{32, 33}$ In the absence of more complicated dynamics behavior, such as conformational exchange, it can be viewed as an integral of ordinary mono-exponential relaxation functions over a distribution of the relaxation rates. 34 We have previously shown that characteristic changes in β can indicate the transition point between two mechanisms contributing to relaxation. $^{35, 36}$ Further, for relaxation involving methyl and phenyl groups in amino acids in proteins $^{35-39}$ we have shown that the inhomogeneity in the local environment can be treated globally across a range of temperatures invoking a distribution in the activation energies of corresponding motions. Thus, the non-exponential behavior at both temperature ends signifies the presence of the distributions of activation energies for the 3-site jump and C^{α} - C^{β} axis fluctuations mechanisms. For the 3-site jumps mode, it is sufficient to introduce only the distribution for the

height of the potential energy barrier between the rotamers, E_a^{3-site} (Figure 4C). Gaussian shapes were assumed and the global fitting for the entire temperature range (see Materials and Methods section for details) yielded the following parameters for the central values and distribution widths: $\langle E_a^{3-site} \rangle = 30.2 \pm 1.7 \, \text{kJ/mol}$ and $\langle E_a^{small} \rangle = 7.5 \pm 0.4 \, \text{kJ/mol}$ the widths of $\sigma_{3-site} = 7.5 \pm 0.6 \, \text{kJ/mol}$ and $\sigma_{small} = 1.9 \pm 0.3 \, \text{kJ/mol}$. As expected, the activation energy for the 3-site-jump motions of C^β deuterons are significantly higher than what is found for methyl deuterons (7-15 kJ/mol) 40,41 $^{35,37-39,42}$ and is comparable with the activation energies of the phenylalanine ring flips. $^{36,43-45}$ The width of the distribution σ_{3-site} is about 25% of the central value and represents a significant inhomogeneity of the local environment. The value of $\Delta E = 8.8 \, \text{kJ/mol}$ was taken as the minimum value necessary to reproduce the rigid spectrum at the highest temperature in the presence of the distributions of 3-site jumps rate constants. At 330 K, the fitted value of ΔE corresponds to the ratio of weights of the major and minor rotamers of 25:1:1. All fitted parameters are summarized in Table 1.

II. S8 in Aβ₁₋₄₀ fibrils

The T_1 relaxation behavior of the S8 site in the dry A β fibrils (Figures 5 and 6) is qualitatively similar to Fmoc-serine and the same motional model of Figure 4A was applied. At high temperatures, the relaxation times are smaller in the fibrils compared to Fmoc-serine, implying faster 3-site jumps. Data at the extreme of the low temperature range are difficult to obtain for the fibril samples due to large relaxation times and much lower sensitivity compared with the Fmoc-serine. As the small-angle fluctuations around the χ_1 dihedral angle are not expected to be affected much by changes in the packing and distant structural changes, it is reasonable to assume that they are the same in all systems considered here. The fits for the dry fibrils were thus performed with

the parameters of the small-angle fluctuations fixed at the values determined for Fmoc -serine. The value of $\Delta E = 8.8$ kJ/mol is also kept the same as in Fmoc-serine, as it is fully consistent with the spectral data for all temperatures and permits for a direct comparison between the two systems. An interesting difference between Fmoc-serine and dry fibrils lies in the width of the distributions, which is $\sigma_{3-site} = 5.0 \pm 0.3$ kJ/mol for the dry fibrils, as compared with $\sigma_{3-site} = 7.5 \pm 0.6$ kJ/mol for Fmoc -serine, indicating that the extent of inhomogeneity of the local environment is reduced in the fibrils. The values of the activation energies are the same in the Fmoc-serine and dry fibrils at 30 kJ/mol, indicating similar restriction of local motions of the C^{β} deuterons. There are also differences in the fitted value of the Arrhenius prefactor k_0^{3-site} , reflecting faster k_0^{3-site} rate constants in the fibrils at high temperatures.

As mentioned in the previous section, in the hydrated fibrils the line shape at high temperature are dominated by the slow large-scale diffusive motion (Figure 4B). The time scale of this motion is much slower than the Larmor frequency and does not provide an efficient relaxation mechanism, thus T_1 times in the hydrated protein at high temperature are still dominated by the local 3-site jumps of C^{β} deuterons. At high temperatures the fraction of the bound state is too small to reliably measure its relaxation times and we can only measure the relaxation times of the narrowed peak corresponding to the free state. For the free state within experimental uncertainty the magnetization build up curves can be fitted with a single exponent (Figure 5). As the temperature is lowered, the fraction of the bound state becomes sufficiently high (Figure 3) to measure differentially the relaxation originating from the free state (central peak) and the bound state (± 53.5 kHz spectral frequencies, corresponding to the horn position of the rigid powder pattern of the bound state). The relaxation times of the two components are orders of magnitude different from each other. This relaxation anisotropy of the free and bound states was also observed for the side-chains of F4, τ -H6 and G9 of the fibrils. τ -Magnetization build-up cures for the wide component of the spectra

originating from the bound state are not single-exponential, unlike what is seen for the build-up curves of the central spectral component. Due to low sensitivity of the signal originating from the bound state it is difficult to obtain the exact extent of non-exponentiality in the magnetization build-up curves reliably. Thus, we performed the fits of the magnetization build-up curves in which the value of β was fixed at 0.65, which roughly corresponds to the values obtained for the dry protein in this regime. Leaving β as a free fitting parameter led to T_1^{eff} values consistent with this assumption but was clearly over-fitting the data.

The spectral position of the major singularities of the bound state at ± 53.5 kHz are consistent with the ΔE value of 8.8 kJ/mol used for the dry fibrils. For the bound state relaxation is in the slow motional regime with respect to the Larmor frequency, i.e. relaxation times increase with decrease in temperature. In analogy to the dry state of the fibrils, we again assume that the small-angle fluctuations remain similar to the case of Fmoc-serine. The width of the distribution of σ_{3-site} was thus assumed to be similar to the dry state and fixed at 5 kJ/mol, consistent with fixing the value of β at 0.65 in the non-exponential relaxation build-up curves. With these assumptions, the global fitting across 272-207 K temperature range with the use of the two mechanisms yields $\langle E_a^{3-site} \rangle = 41.7 \pm 2$ kJ/mol.

In contrast, for the free state of the hydrated fibrils the *T*₁ relaxation times are in the fast motional regime with respect to the Larmor frequency (i.e., relaxation times decreases with decrease in temperature), indicating that the 3-site jumps mechanism is dominant and the small-angle fluctuations can be neglected. Note, that the last point at 220 K already starts to exhibit sings of the sigmoidal rise of the relaxation times, which was also characteristic of the side-chains of F4, τ-H6 and G9 in the temperature regime when the fraction of the free state is very small. Thus, for the free state the activation energy for the 3-site jumps mode was obtained by first fitting the rate constants at individual temperatures and then fitting the temperature dependence in the 302 –

240 K temperature range to the Arrhenius Law, without invoking the assumption of the distribution of the activation energies due to the single-exponential nature of the magnetization build-up curves. For the free state the data indicate that the three rotameric populations of the C^{β} deuterons remain roughly equivalent. If a preferential population is assumed in analogy to the bound state, the relaxation times at temperatures below about 275 K cannot be fitted, because the minimum achievable value of T_1 is much higher than what is observed experimentally. As stated in the "Sample conditions, labeling patterns, and spectral analysis" section above, further corroboration of the nearly equal rotameric populations is seen from the high temperature spectrum. The resulting value of $E_a^{3-site} = 25.6$ kJ/mol for the free state of the hydrated fibrils is significantly smaller than $\langle E_a^{3-site} \rangle = 41.7 \pm 2 \text{ kJ/mol}$ for the bound state, indicating that the C^{\beta} 3-site jumps of S8 are less restricted in the free state of the hydrated fibrils compared to the bound state. However, within the error limits $E_a^{3-site} = 25.6 \pm 1$ kJ/mol for the free state is not that different from the $\langle E_a^{3-site} \rangle = 30$ ±2 kJ/mol for the dry state of the fibrils. Finally, to compare the actual rate constants for the 3-site jumps at high temperatures close to physiological condition, we calculate their values within one standard deviation of the Gaussian distribution of the activation energies at 300 K. The free state of the hydrated fibrils has the highest typical value of $k^{3\text{-site}}$ (300 K) = 8.5·10⁹ s⁻¹, followed in the decreasing order by the bound state of the hydrated fibrils with the central value of 1.9·10⁸ s⁻¹ (with the range of $5.1 \cdot 10^7$ to $6.8 \cdot 10^9$ s⁻¹), the dry state of the hydrated fibrils $6.9 \cdot 10^7$ s⁻¹ (with the range of $1.7 \cdot 10^7$ to $2.5 \cdot 10^8$ s⁻¹), and Fmoc-serine $1.3 \cdot 10^6$ s⁻¹ (with the range of $6.3 \cdot 10^4$ to $2.7 \cdot 10^6$ s⁻¹).

In general, the enhanced mobility of the N-terminal domain of the fibrils in the hydrated state and the existence of the dynamic equilibrium between the free and bound states of the fibrils is in line with several other dynamics studies. Methyl jumps occurring at faster rates can serve as precursors to the onset of slower time scales modes such the diffusive motion of the N-terminal domain and conformational exchange between free and bound states. Of particular relevance are

studies of mature fibrils by of A β fibrils by Huster and coworkers, ²⁰ as well as the studies of binding of monomeric A β to the surface of protofibrils by Fawzi and coworkers, ⁴⁶ who utilized solution NMR dark saturation transfer approaches. They modeled the exchange dynamics with kinetic schemes involving two to three states, corresponding to the free monomer and the monomer–protofibril complexes with a differential extent of mobility. Further, a recent work of Rezaei-Ghaleh et al.⁴⁷ using an integrated approach from ¹⁵N NMR relaxation rates, nanosecond fluorescence correlation spectroscopy, and MD simulations indicated the presence of slow segmental motions in A β monomers on the time scales of several nanoseconds. They suggested that aggregation behavior of A β can be controlled through a subtle balance between the characteristic times of intra- and intermolecular diffusion and internal dynamics of A β . Thus, the existence of mobile states of the N-terminal domain undergoing transient interactions with the structured hydrophobic core could be a general property of the A β ensemble of monomers, protofibrils, oligomers, and fibrils and one of the ways of aggregation control pathways.

Conclusion

In the hydrated state the S8 side-chain of the fibrils shows the presence of two states: the free state undergoing large-scale diffusion motions and the bound state in which these motions are quenched. These qualitative results, as well as the values of fitted parameters of the diffusion coefficients and the fraction of the bound state, are well in line with the corresponding values found for other residues in the N-terminal domain of the fibrils.¹⁹

At the physiological temperature, the free state dominates the spectrum of the hydrated fibrils, leading to a pronounced central component, in sharp contrast to either the dry fibrils or Fmoc - Serine amino acid, both of which display the spectra with characteristics of the rigid powder pattern. Longitudinal relaxation rates are dominated by the local motions consisting of the 3-site

rotameric jumps of the C^{β} deuterons at high temperature and small-angle fluctuations around the χ_1 dihedral angle at lower temperatures. While in Fmoc-serine, the dry fibrils, and the bound state of the hydrated fibrils the rotameric populations at the C^{β} position are clearly unequal, in the free state of the hydrated fibrils they are comparable, probably due to the less dense local packing. A detailed analysis of the relaxation data across a wide temperature range led to the determination of the activation energies of the local modes. The value of $\langle E_a^{3-site} \rangle$ is the largest for the bound state of the fibrils (42 kJ/mol), followed by values in the 26-30 kJ/mol range for all other systems. As expected, these values are also considerably larger than the typical activation energy for methyl 3site jumps. Two additional interesting features can be detected in Fmoc-serine, dry fibrils, and the bound state of the hydrated fibrils: inhomogeneity effects of the local environment, which manifest in the non-exponential behavior of the magnetization build-up curves and can be modeled with the distributions of the activation energies for both of the motional mechanisms. For the 3-site jump mechanism the widths of these distributions are around 7.5 kJ/mol for Fmoc-serine and 5 kJ/mol for the dry fibrils and the bound state of the wet fibrils, pointing to the fact that the inhomogeneity is less pronounced in the fibrils compared to the serine amino acid. Interestingly, within the experimental precision the distribution is entirely absent in the free state of the hydrated fibrils. which is possibly due to the averaging of the environment in the presence of the large-scale diffusion mode. Also in the free state of the fibrils the rate constants are orders of magnitude faster than in all other systems and are in the fast limit with respect to the Larmor frequency. For all other systems they are in the slow motional regime. At 300 K the typical rate constants value decrease from the free state of the hydrated fibrils (8.5·10⁹ s⁻¹), to the bound state of the hydrated fibrils $(1.9 \cdot 10^8 \,\mathrm{s}^{-1})$, followed by the dry fibrils $(16.9 \cdot 10^7 \,\mathrm{s}^{-1})$, and finally Fmoc-serine $(1.3 \cdot 10^6 \,\mathrm{s}^{-1})$.

Lastly, our study of serine side-chains was motivated by the potential for the regulation of aggregation control of the fibrils at the S8 site via phosphorylation^{15, 16, 48} and general involvement

of serine side-chains in post-translational modifications. This work established approaches for studies of the dynamics of serine side-chains in a variety of systems and environments, as well as provided the expected ranges of parameters and motional mechanisms. The specifics depend on structural details, the hydration state of the system, and the temperature range of interest. A particularly promising future direction is application to phosphorylated serine side-chains, which are common post-translational modifications in biological systems.

Acknowledgements

This work was supported by a National Institutes of Health Grant 1R15-GM111681 and NSF grant 1726947. D.R. was supported by CU Denver undergraduate research grant. This study made use of the Campus Chemical Instrument Center NMR facility at Ohio State University.

Supporting Information Available

Synthetic procedures for preparation Fmoc-serine-Trt-d₃ (SI1 and Figure S1). Decomposition of the high temperature spectrum into the components corresponding to the bound and free states in hydrated A β and fits to the isotropic diffusion model (Figure S2). Spectra corresponding to $k^{3\text{-site}}$ with equal populations fits at the highest temperature for Fmoc-serine (Figure S3). This information is available free of charge via the Internet at http://pubs.acs.org.

Table 1. Summary of fitted parameters according to the model of Figure 4A based on the longitudinal relaxation data of serine C^{β} deuterons.

| sample | $\langle E_a^{3-site} \rangle$, kJ/mol | σ _{3-site} , kJ/mol | $\langle E_a^{small} \rangle$, kJ/mol | σ _{small} , kJ/mol | k_o^{3-site} , s ⁻¹ | k_o^{small} , s ⁻¹ | ΔE , kJ/mol |
|-----------------------------|---|---------------------------------|--|--------------------------------|----------------------------------|---------------------------------|---------------------|
| Fmoc-serine | 30.2 ±1.7 | 7.5 ±0.6 | 7.5 ±0.4 | 1.9±0.3 | 2.3 ·10 11 | 1.1 ·10 8 | 8.8±0.2 |
| Dry fibrils S8 | 30.0 ±2.0 | 5.0 ±0.3 | fixed at 7.5 | fixed at 1.9 | 5.8 ·10 11 | fixed at | 8.8±0.2 |
| | | | | | | 1.1 ·10 8 | |
| Wet fibrils S8, bound state | 41.7 ±2.0 | fixed at 5.0 | fixed at 7.5 | fixed at 1.9 | 3.5 ·10 ¹⁵ | fixed at | 8.8±0.2 |
| | | | | | | 1.1 ·10 8 | |
| Wet fibrils S8, free state | 25.6 ±1.0 | not used | not used | not used | 2.5 ·10 ¹⁴ | not used | 0 |

References

- (1) Petkova, A. T.; Leapman, R. D.; Guo, Z. H.; Yau, W. M.; Mattson, M. P. and Tycko, R. Self-Propagating, Molecular-Level Polymorphism in Alzheimer's Beta-Amyloid Fibrils *Science* **2005**, *307*, 262-265.
- (2) Colvin, M.; Silvers, R.; Ni, Z. Q.; Can, T. V.; Sergeyev, I.; Rosay, M.; Donovan, K. J.; Michael, B.; Wall, J.; Linse, S. et al. Atomic Resolution Structure of Monomorphic Aβ42 Amyloid Fibrils *J. Am. Chem. Soc.* **2016**, *138*, 9663–9674.
- (3) Luhrs, T.; Ritter, C.; Adrian, M.; Riek-Loher, D.; Bohrmann, B.; Doeli, H.; Schubert, D. and Riek, R. 3d Structure of Alzheimer's Amyloid-Beta(1-42) Fibrils *Proc. Natl. Acad. Sci. U.S.A.* **2005**, *102*, 17342-17347.
- (4) Hardy, J. and Selkoe, D. J. The Amyloid Hypothesis of Alzheimer's Disease: Progress and Problems on the Road to Therapeutics *Science* **2002**, *297*, 353-356.
- (5) Hamley, I. W. The Amyloid Beta Peptide: A Chemist's Perspective. Role in Alzheimer's and Fibrillization *Chem. Rev.* **2012**, *112*, 5147-5192.
- (6) Musiek, E. S. and Holtzman, D. M. Three Dimensions of the Amyloid Hypothesis: Time, Space and 'Wingmen' *Nat. Neurosci.* **2015**, *18*, 800-806.
- (7) Mazzitelli, S.; Filipello, F.; Rasile, M.; Lauranzano, E.; Starvaggi-Cucuzza, C.; Tamborini, M.; Pozzi, D.; Barajon, I.; Giorgino, T.; Natalello, A. et al. Amyloid-B 1–24 C-Terminal Truncated Fragment Promotes Amyloid-B 1–42 Aggregate Formation in the Healthy Brain *Acta. Neuropath. Commun.* **2016**, *4*, 110-115.
- (8) Brannstrom, K.; Ohman, A.; Nilsson, L.; Pihl, M.; Sandblad, L. and Olofsson, A. The N-Terminal Region of Amyloid Beta Controls the Aggregation Rate and Fibril Stability at Low Ph through a Gain of Function Mechanism *J. Am. Chem. Soc.* **2014**, *136*, 10956-64.
- (9) Morris, C.; Cupples, S.; Kent, T. W.; Elbassal, E. A.; Wojcikiewicz, E. P.; Yi, P. and Du, D. N-Terminal Charged Residues of Amyloid-Beta Peptide Modulate Amyloidogenesis and Interaction with Lipid Membrane *Chemistry* **2018**, *24*, 9494-9498.
- (10) Nussbaum, J. M.; Schilling, S.; Cynis, H.; Silva, A.; Swanson, E.; Wangsanut, T.; Tayler, K.; Wiltgen, B.; Hatami, A.; Ronicke, R. et al. Prion-Like Behaviour and Tau-Dependent Cytotoxicity of Pyroglutamylated Amyloid-Beta *Nature* **2012**, *485*, 651-5.
- (11) Kummer, M. P.; Hermes, M.; Delekarte, A.; Hammerschmidt, T.; Kumar, S.; Terwel, D.; Walter, J.; Pape, H. C.; Konig, S.; Roeber, S. et al. Nitration of Tyrosine 10 Critically Enhances Amyloid Beta Aggregation and Plaque Formation *Neuron*. **2011**, *71*, 833-44.

- (12) Rezaei-Ghaleh, N.; Amininasab, M.; Kumar, S.; Walter, J. and Zweckstetter, M. Phosphorylation Modifies the Molecular Stability of Beta-Amyloid Deposits *Nat. Commun.* **2016**, 7, 11359.
- (13) Xu, L.; Nussinov, R. and Ma, B. Allosteric Stabilization of the Amyloid-B Peptide Hairpin by the Fluctuating N-Terminal *Chem. Commun.* **2016**, *52*, 1733-1736.
- (14) Hubin, E.; van Nuland, N. A. J.; Broersen, K. and Pauwels, K. Transient Dynamics of a Beta Contribute to Toxicity in Alzheimer's Disease *Cell. Mol. Life Sci.* **2014**, *71*, 3507-3521.
- (15) Kummer, M. P. and Heneka, M. T. Truncated and Modified Amyloid-Beta Species *Alzheim*. *Reser. Ther.* **2014**, *6*.
- (16) Hu, Z. W.; Vugmeyster, L.; Au, D. F.; Ostrovsky, D.; Sun, Y. and Qiang, W. The Molecular Structure of a "Seeding-Prone" N-Terminal Phosphorylated B-Amyloid Fibril *Proc. Natl. Acad. Sci. U.S.A.* **2019**, *116*, 11253-11258.
- (17) Paravastu, A. K.; Qahwash, I.; Leapman, R. D.; Meredith, S. C. and Tycko, R. Seeded Growth of Beta-Amyloid Fibrils from Alzheimer's Brain-Derived Fibrils Produces a Distinct Fibril Structure *Proc. Natl. Aca. Sci. U.S.A.* **2009**, *106*, 7443-7448.
- (18) Vugmeyster, L.; Au, D. F.; Ostrovsky, D. and Fu, R. Deuteron Solid-State NMR Relaxation Measurements Reveal Two Distinct Onformational Exchange Processes in the Disordered N-Terminal Domain of Amyloid-B Fibrils *ChemPhysChem.* **2019**, *20*, 1680.
- (19) Au, D. F.; Ostrovsky, D.; Fu, R. and Vugmeyster, L. Solid-State NMR Reveals a Comprehensive View of the Dynamics of the Flexible, Disordered N-Terminal Domain of Amyloid-B Fibrils *J. Biol. Chem.* **2019**, *294*, 5840–5853.
- (20) Scheidt, H. A.; Morgado, I.; Rothemund, S. and Huster, D. Dynamics of Amyloid Beta Fibrils Revealed by Solid-State NMR *J. Biol. Chem.* **2012**, *287*, 2017-2021.
- (21) Krawczyk, B.; Ensle, P.; Muller, W. M. and Sussmuth, R. D. Deuterium Labeled Peptides Give Insights into the Directionality of Class Iii Lantibiotic Synthetase Labke *J. Am. Chem. Soc.* **2012**, *134*, 9922-5.
- (22) Petkova, A. T.; Yau, W. M. and Tycko, R. Experimental Constraints on Quaternary Structure in Alzheimer's Beta-Amyloid Fibrils *Biochemistry* **2006**, *45*, 498-512.
- (23) Vold, R. L. and Vold, R. R. Deuterium Relaxation in Molecular Solids. In *Advances in Magnetic and Optical Resonance*; Warren, W. Ed.; Acadenic Press: San Diego, 1991, pp 85-171.
- (24) Persson, P.-O. and Strang, G. A Simple Mesh Generator in Matlab *SIAM Rev.* **2004**, *46*, 329-345.
- (25) Duer, M. J. Solid-State NMR Spectroscopy, Blackwell Publishing Ltd: Oxford, 2004.

- (26) Torchia, D. A. and Szabo, A. Spin-Lattice Relaxation in Solids *J. Magn. Reson.* **1982**, *49*, 107-121.
- (27) Vugmeyster, L.; Ostrovsky, D. and Lipton, A. S. Origin of Abrupt Rise in Deuteron NMR Longitudinal Relaxation Times of Protein Methyl Groups Below 90 K *J. Phys. Chem. B* **2013**, *117*, 6129-6137.
- (28) Binev, Y.; Marques, M. M. B. and Aires-de-Sousa, J. Prediction of 1h NMR Coupling Constants with Associative Neural Networks Trained for Chemical Shifts *J. Chem. Info. Model.* **2007**, *47*, 2089-2097.
- (29) Shapovalov, M. V. and Dunbrack, R. L.; Jr. A Smoothed Backbone-Dependent Rotamer Library for Proteins Derived from Adaptive Kernel Density Estimates and Regressions *Structure* **2011**, *19*, 844-858.
- (30) Dunbrack, R. L.; Jr. and Cohen, F. E. Bayesian Statistical Analysis of Protein Side-Chain Rotamer Preferences *Prot. Sci.* **1997**, *6*, 1661-81.
- (31) Beckmann, P. A. and Schneider, E. Methyl Group Rotation, H-1 Spin-Lattice Relaxation in an Organic Solid, and the Analysis of Nonexponential Relaxation *J. Chem. Phys.* **2012**, *136*, 054508.
- (32) Sillescu, H. Heterogeneity at the Glass Transition: A Review J. NonCryst. Sol. 1999, 243, 81-108.
- (33) Schnauss, W.; Fujara, F.; Hartmann, K. and Sillescu, H. Nonexponential H-2 Spin-Lattice Relaxation as a Signature of the Glassy State *Chem.Phys. Lett.* **1990**, *166*, 381-384.
- (34) Lindsey, C. P. and Patterson, G. D. Detailed Comparison of the Williams-Watts and Cole-Davidson Functions *J. Chem. Phys.* **1980**, *73*, 3348-3357.
- (35) Vugmeyster, L.; Ostrovsky, D.; Penland, K.; Hoatson, G. L. and Vold, R. L. Glassy Dynamics of Protein Methyl Groups Revealed by Deuteron NMR *J. Phys. Chem. B* **2013**, *117*, 1051-1061.
- (36) Vugmeyster, L.; Osrovsky, D.; Villafranca, T. R.; Sharp, J.; Xu, W.; Lipton, A. S.; Hoatson, G. L. and Vold, R. L. Dynamics of Hydrophobic Core Phenylalanine Residues Probed by Solid-State Deuteron NMR *J. Phys. Chem. B.* **2015**, *119*, 14892–14904.
- (37) Vugmeyster, L. and Ostrovsky, D. Static Solid-State 2H NMR Methods in Studies of Protein Side-Chain Dynamics *Prog. Nucl. Magn. Reson. Spec.* **2017**, *101*, 1-17.
- (38) Vugmeyster, L. and Ostrovsky, D. Comparative Dynamics of Methionine Side-Chain in Fmoc-Methionine and in Amyloid Fibrils *Chem. Phys. Lett.* **2017**, *673*, 108-112.
- (39) Vugmeyster, L.; Ostrovsky, D.; Clark, M. A.; Falconer, B. I.; Hoatson, G. L. and Qiang, W. Fast Motions of Key Methyl Groups in Amyloid-Beta Fibrils *Biophys. J.* **2016**, *111*, 2135-2148.

- (40) Batchelder, L. S.; Niu, C. H. and Torchia, D. A. Methyl Reorientation in Polycrystalline Amino-Acids and Peptides a H-2 NMR Spin-Lattice Relaxation Study *J. Am. Chem. Soc.* **1983**, *105*, 2228-2231.
- (41) Batchelder, L. S.; Sullivan, C. E.; Jelinski, L. W. and Torchia, D. A. Characterization of Leucine Side-Chain Reorientation in Collagen Fibrils by Solid-State H-2 NMR *Proc. Natl. Acad. Sci. U. S. A.* **1982**, *79*, 386-389.
- (42) Vugmeyster, L.; Ostrovsky, D.; Khadjinova, A.; Ellden, J.; Hoatson, G. L. and Vold, R. L. Slow Motions in the Hydrophobic Core of Chicken Villin Headpiece Subdomain and Their Contributions to Configurational Entropy and Heat Capacity from Solid-State Deuteron NMR Measurements *Biochemistry* **2011**, *50*, 10637–10646.
- (43) Hiyama, Y.; Silverton, J. V.; Torchia, D. A.; Gerig, J. T. and Hammond, S. J. Molecular-Structure and Dynamics of Crystalline Para-Fluoro-D,L-Phenylalanine a Combined X-Ray NMR Investigation *J. Am. Chem. Soc.* **1986**, *108*, 2715-2723.
- (44) Vugmeyster, L.; Ostrovsky, D.; Hoatson, G. L.; Qiang, W. and Falconer, B. I. Phenylalanine Side-Chain in the Hydrophobic Core of Amyloid Fibrils Reveals a Solvent-Driven Dynamical Transition. *J. Phys. Chem. B* **2017**, *121*, 7267–7275.
- (45) Gall, C. M.; Cross, T. A.; Diverdi, J. A. and Opella, S. J. Protein Dynamics by Solid-State NMR Aromatic Rings of the Coat Protein in Fd Bacteriophage *Proc. Natl. Acad. Sci. U. S. A.* **1982**, *79*, 101-105.
- (46) Fawzi, N. L.; Ying, J.; Ghirlando, R.; Torchia, D. A. and Clore, G. M. Atomic-Resolution Dynamics on the Surface of Amyloid-Beta Protofibrils Probed by Solution NMR *Nature* **2011**, *480*, 268-72.
- (47) Rezaei-Ghaleh, N.; Parigi, G. and Zweckstetter, M. Reorientational Dynamics of Amyloid-B from NMR Spin Relaxation and Molecular Simulation *J. Phys. Chem. Lett.* **2019**, *10*, 3369-3375.
- (48) Hu, Z.-W.; Ma, M.-R.; Chen, Y.-X.; Zhao, Y.-F.; Qiang, W. and Li, Y.-M. Phosphorylation at Ser8 as an Intrinsic Regulatory Switch to Regulate the Morphologies and Structures of Alzheimer's 40-Residue B-Amyloid (Aβ40) Fibrils *J. Biol. Chem.* **2017**, *292*, 2611-2623.
- (49) Paravastu, A. K.; Leapman, R. D.; Yau, W. M. and Tycko, R. Molecular Structural Basis for Polymorphism in Alzheimer's Beta-Amyloid Fibrils *Proc. Natl. Aca. Sci. U.S.A.* **2008**, *105*, 18349-18354.

Figures

Figure 1. A) The structure of Fmoc-L-serine- $C^{\alpha}D$ - $C^{\beta}D_2$. B) Monomeric unit of the 3-fold symmetric structure of $A\beta_{1-40}$ fibrils, indicating schematically the position of the S8 site belonging to the N-terminal subdomain (residues 1-16). The structural coordinates (PDB ID 2LMP.pdb)⁴⁹ start with residue 9 and the rest of the N-terminal domain is shown schematically. C) The 3-fold symmetric fibril structure, top view.⁴⁹ D) A typical example of a negatively stained transmission electron microscopy image of the fibrils used in this work.

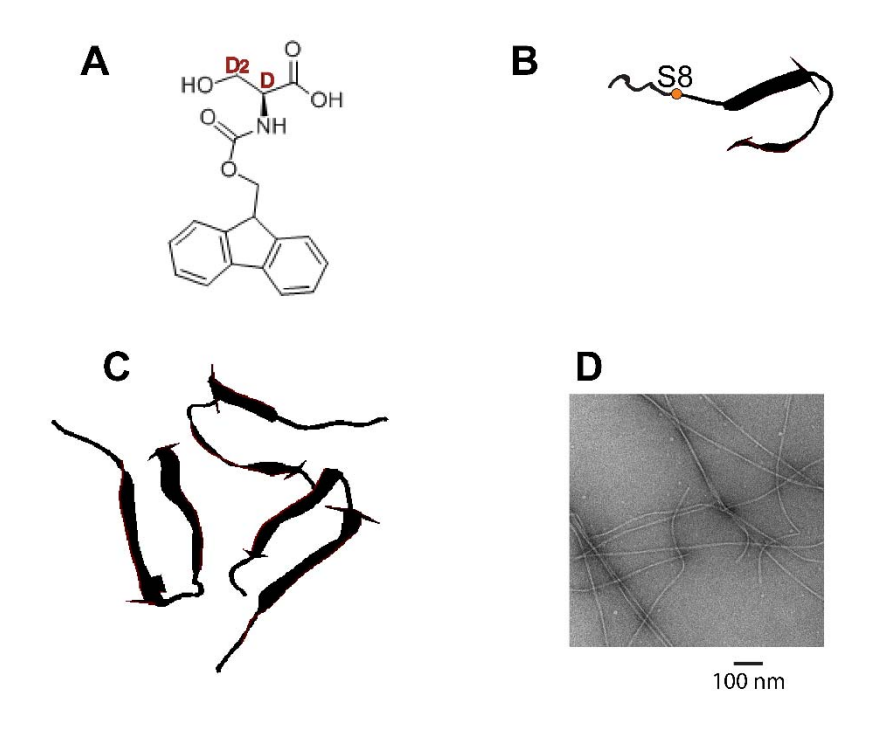


Figure 2. Fmoc-serine- $C^{\alpha}D$ - $C^{\beta}D_2$ ²H NMR measurements at 18.8 T and MAS rate of 25 kHz at 313 K. A) normalized spectra of the central band with inter-scan delays of 1s (red line) and 10 min (black line).

Exponential line broadening of 1 Hz was employed. B) T_1 relaxation times showing a negligible extent of anisotropy of the central band region (single exponential fits).

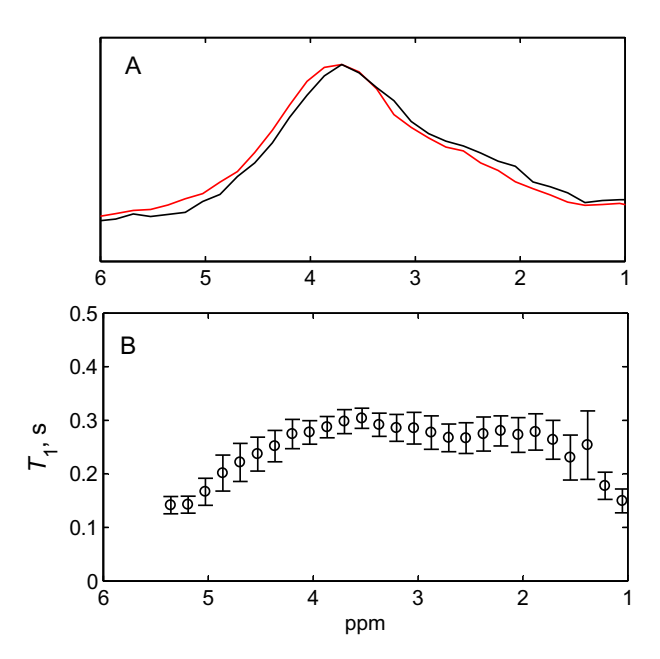


Figure 3. ²H NMR line shapes under static conditions recorded at 9.4 T with the use of the quadrupolar echo experiment for A) Fmoc-serine $C^{\alpha}D$ $C^{\beta}D_2$ at 310 K, indicating a rigid-like powder pattern; B) S8- $C^{\alpha}D$ $C^{\beta}D_2$ of $A\beta_{1-40}$ fibrils in dry state at the highest measured temperature of 302 K; C) S8- $C^{\alpha}D$ $C^{\beta}D_2$ of $A\beta_{1-40}$ in the hydrated state at 310 K and D) at 263 K. The insert for the 310 K spectrum of the hydrated fibrils shows magnification of the baseline, in which the rigid component corresponding to the bound state is visible. The central peak at zero frequency corresponds to the free state. As the temperature is lowered the fraction of the rigid pattern in the hydrated state increases, indicating the freezing of the large-scale diffusive motions.

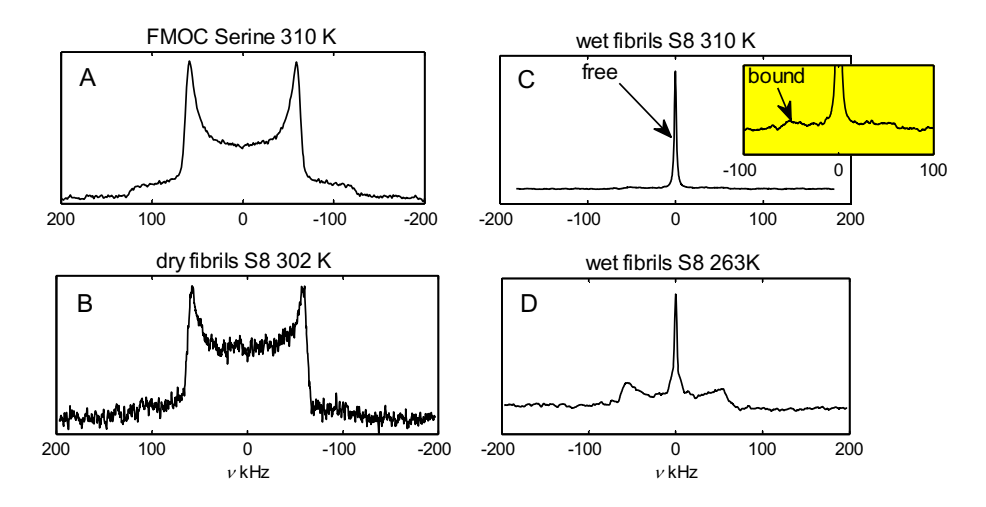


Figure 4. Motional model A) Local modes of the serine side-chain: 3-site jump of C^{β} deuterons according to the tetrahedral geometry and involving rearrangements of the two deuterons and the -OH group are shown with the curved double-sided arrows with the corresponding rate constant $k^{3-\text{site}}$. One major and two minor populations of the three exchanging sites are assumed to be in the w:1:1 ratio. An additional mode of small-angle fluctuations takes place along the same χ_1 angle with the rate constant k_{small} . B) The two-state motional model for the global motion of the N-terminal subdomain in the hydrated fibrils (residues 1-16 of $A\beta_{1-40}$) at 37°C determined from previous work: ^{18, 19} the N-terminal domain is shown as the curved line with the position of S8 site as an orange dot, while the C-terminal subdomain is shown as a blue rectangle. In the free state (left) the domain undergoes a large-scale diffusive motion (with the isotropic diffusion coefficient D), which is represented by the gray sphere. In the bound state (right) the diffusion is quenched due to inter- and intra-molecular interactions. The two states are in the slow conformational exchange. The diffusive motion defines the line shapes at the S8 site, while T_1 relaxation is governed by the local modes depicted in part A). C) Potential which includes the local motional modes of the 3-site jumps and small-angle fluctuations around the C^{α} - C^{β} axis. The activation energy barrier E_a^{3-site} corresponds to jumps between one major and two equivalent minor conformers (with the energy difference ΔE) and E_a^{small} corresponds to the energy barrier for the small-angle fluctuations, modeled with the 10° amplitude. The x-axis shows relative changes of χ_1 . The full model for Fmoc-serine, dry fibrils, and the bound state of the free fibrils also involves the Gaussian distributions of the two activation energies. The distribution of E_a^{3-site} is absent in the free state of the hydrated fibrils and $\Delta E = 0$.

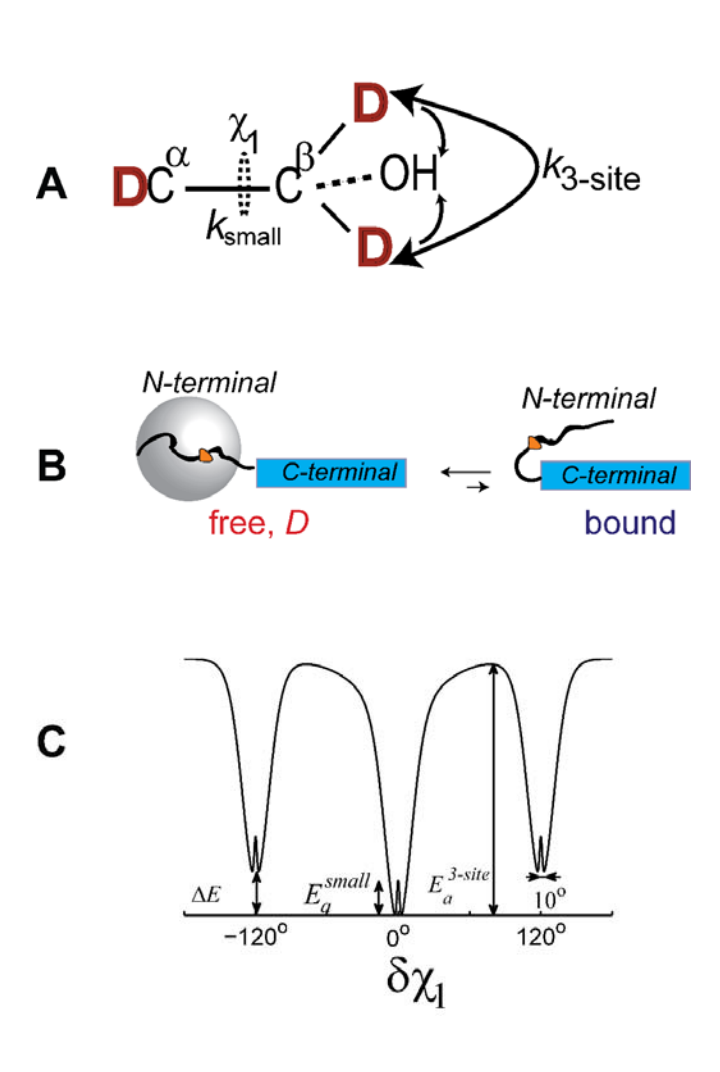


Figure 5. Examples of 2 H NMR longitudinal relaxation magnetization build up curves M(t) in arbitrary units, obtained under static solid-state conditions at 9.4 T for the C^β deuterons of Fmoc-serine and the S8 site of Aβ₁₋₄₀ fibrils. Intensities were taken at the horn positions (i.e., the major singularities) of the powder pattern for Fmoc-serine and dry fibrils, while for the hydrated fibrils intensities were taken for the free state at the central spectral component of 0 kHz, or the horn positions of the rigid fraction corresponding to \pm 53-58 kHz ranges. The red lines represent the fits to the stretched exponential function of Eq. (3). The black lines represent single exponential fits.

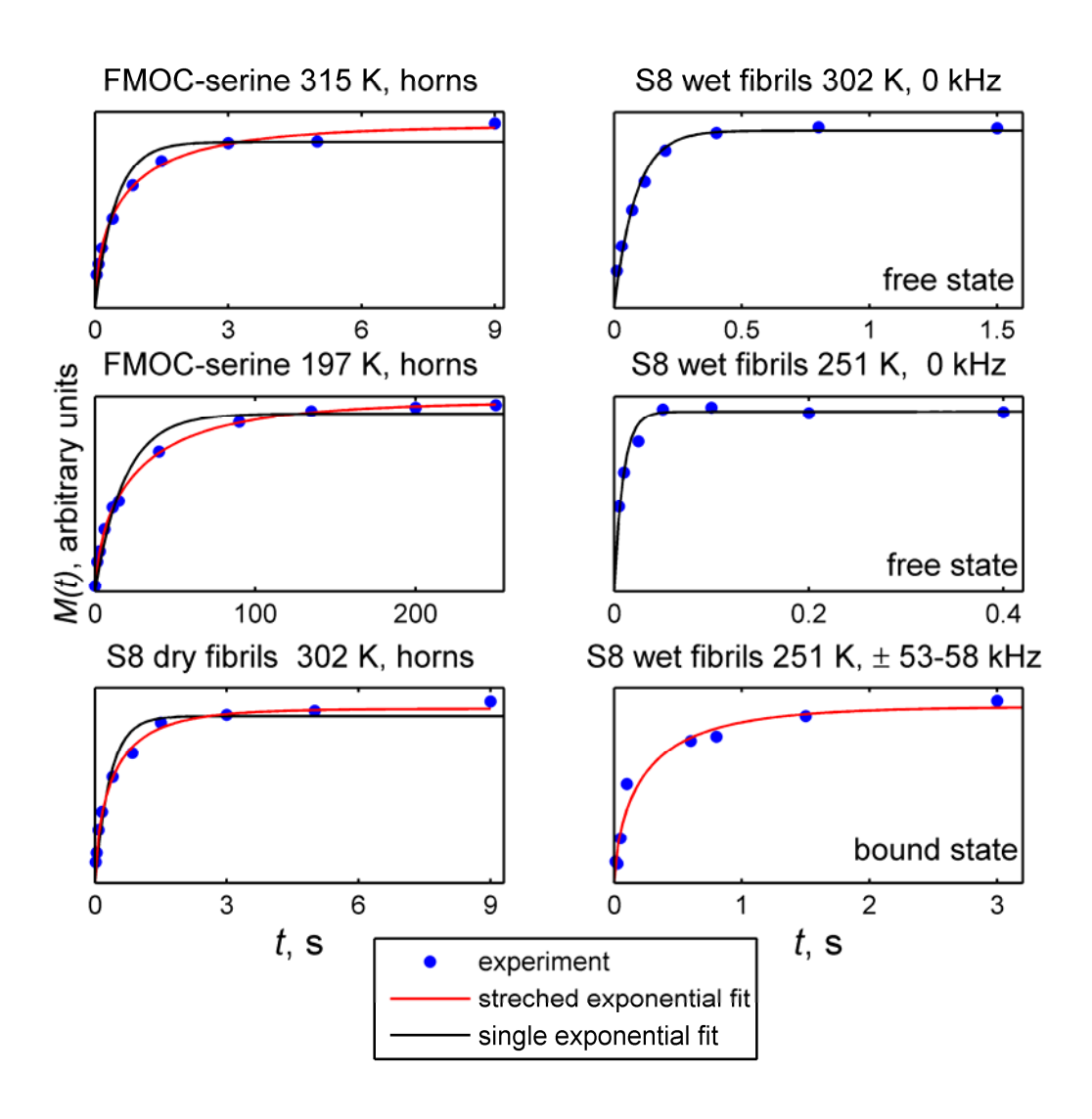
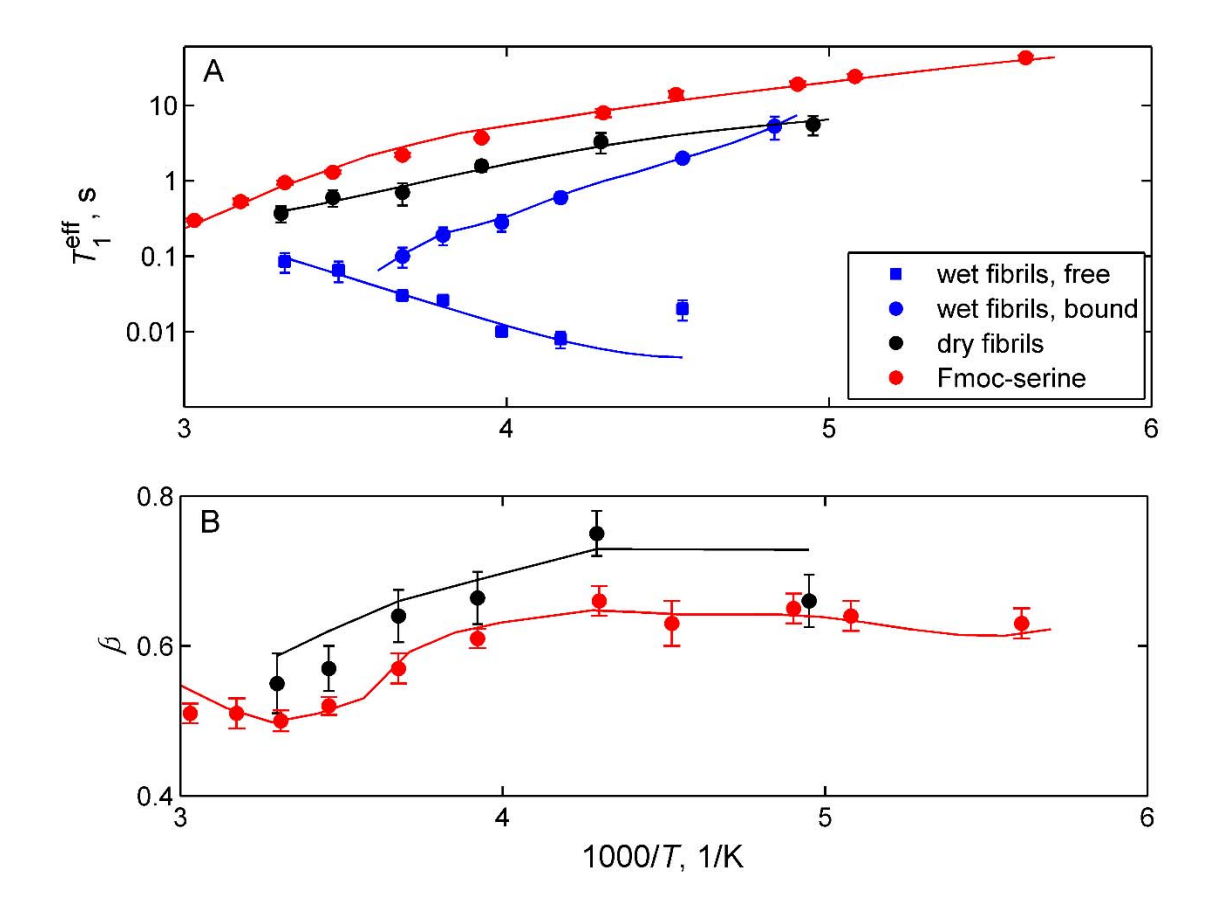


Figure 6. A) ²H NMR longitudinal relaxation times T_1^{eff} (for the stretched exponential fits of Eq. 3) or T_1 (for the single exponential fits) and B) β versus 1000/T. For Fmoc-serine and the S8 site in the dry $A\beta_{1-40}$ fibrils all fits have been performed according to Eq. 3. For the S8 site in the hydrated fibrils the single exponential fits were used for the central component, corresponding to the free state of the fibrils depicted in Figure 4B, and the stretched-exponential fits with β fixed at 0.65 were used for the \pm 53-58 kHz spectral region corresponding to the bound state of the fibrils. The lines represent the fits to the data according to the modeling procedures described in the text.



TOC

